Journal of the European Ceramic Society 20 (2000) 2447–2455

Surface machining of fine-grain Y-TZP

H.C. Kao, F.Y. Ho, C.C. Yang, W.J. Wei *

Institute of Materials Science and Engineering, National Taiwan University, 1 Roosevelt Road, Section 4, Taipei, Taiwan 106, ROC

Received 27 November 1999; received in revised form 13 March 2000; accepted 18 March 2000

Abstract

The effects of diamond wheel grinding on dense (99.7% theoretical density), fine grain (0.38 μm) 3Y-TZP were investigated under various grinding conditions and after annealing temperatures at 1100 to 1300°C for the surface refinement. Scratching test was also used to simulate the interactions of the diamond grit with the TZP. The scratching tracks on the ground surface and the resulted cracks in the subsurface were observed by scanning and transmission electron microscopy (SEM and TEM). The results illustrated the features of plastic deformation, radial crack, median crack, and processing zone. The surfaces were also examined by X-ray diffraction (XRD) which indicated the formation of monoclinic phase, rhombohedral phase (r-phase), and ferroelastic domain switching (FDS). The heat treatment contributed the refinement of surface grains resulted in a reduction of average size from 0.38 to 0.15 μm. Microstructural observation, grinding force measurement, and flexural strength measurement indicate that appropriate grinding parameters are capable of preventing the formation of large defects and retaining the mechanical properties of TZP.

Keywords: Grinding; Mechanical properties; Plastic deformation; Scratching; ZrO_2

1. Introduction

In order to control the dimension and surface quality of ceramic products, a machining process can hardly be avoided. Grinding with a diamond wheel is the most popular process for the shaping and dimensional control of advanced ceramics. The grinding process will cause a processing zone (i.e. the plastic deformation, phase transformation or microcracks zone) and may result in machining defects on the surface and subsurface (i.e. the zone just under ground surface).[1–6] The formation of machining defects depends on the grinding parameters and material properties. For brittle ceramics, the porosity zone,[4] surface cracks,[5] grain pull-out,[7] grooves[3,5,7,8] and bulges[4,9] appear frequently on the ground surface. Subsurface machining defects, such as median cracks,[7,8] lateral cracks,[7,8] twin/slip bands,[7] and microcracks[5,7,8] are observed and reported in literature.

Machining defects are formed due to various material removal mechanisms. The grooves, bulges and twin/slip bands are caused by plastic deformation mechanisms and the others result from brittle fracture. Since cracks and other machining defects can be responsible for the strength degradation of ceramics,[5,10,11] the machining induced plastic deformation of the surface is preferable.

Because of the excellent mechanical properties, the zirconia has been widely studied. In addition to the transformation of the tetragonal (t) to monoclinic (m) phase, the formation of rhombohedral phase (r-phase),[12,13] and ferroelastic domain switching (FDS)[14,15] were observed on the ground surface. The X-ray diffraction (XRD) peak of (111) of t-phase [abbreviated as $(111)_t$][2] ZrO_2 was in different shapes before and after grinding.[12] Hasegawa[12] calculated that the strongest diffraction peak of r-phase is $(111)_r$ ($2\theta = 29.57°$) which was very close to the $(111)_t$ and would make the $(111)_t$ peak non-symmetrical. However, after aging at 250°C for 120 h, the $(111)_t$ peak became symmetrical again. Kim et al.[13] also observed this phenomenon on ground surfaces of 3Y-TZP and 12Ce-TZP.

The ferroelastic domain switch (FDS) has been identified by the reversal of the $(002)_t$ and $(200)_t$ intensities in the XRD pattern.[14,15] Virkar et al.[14] reported that the grinding process or compressive stress will change the ratio of intensities of the $(002)_t$ and $(200)_t$ peaks, indicated by $(I_{(002)t}/I_{(200)t})$. For sintered or polished surfaces,

* Corresponding author. Tel.: +886-2263-0231, ext. 2701; fax: +886-22363-4562.

E-mail address: wjwei@ccms.ntu.edu.tw (J. Wei).

0955-2219/00/$ - see front matter
PII: S0955-2219(00)00114-X

$I_{(002)t}/I_{(200)t}$ is smaller than one. After grinding, $I_{(002)t}/I_{(200)t}$ is larger than one and decreases with the depth with respect of the ground surface. According to the report by Kitano et al.,[15] machining stress is likely to induce FDS more easily than heat treatment does.

In order to understand the fundamentals of surface microstructure changed by the machining of hard diamond particles, dense tetragonal zirconia polycrystalline (TZP) were wheel ground and examined extensively by different microscopic techniques. The effects of grinding parameters and heat treatment on the surface properties were also investigated.

2. Experimental procedure

Polycrystalline zirconia samples were prepared from a commercially available zirconia powder (TZ3Y, Tosoh, Japan). Colloidal processing was adopted to form green bodies with a cylindrical shape of 70 mm diameter and 6–7 mm thickness. After sintering at 1480°C for 1 h with the ramping rate 10°C/min and cooling rate 30°C/min, the relative density and average grain size measured by Archimedes' method and linear intersection method were 99.7% theoretical density (TD) and 0.38 μm, respectively.

The sintered samples were ground with diamond wheels (#220, #325 or #800 grid size) by a creep-feed surface grinder (KCF-52AHD, Kent, Taiwan). All wheels are in a concentration of 100 (4.4 ct/cm^3). The tangential speed of the wheel is 1310 m/min and the relative moving speed of TZP samples are 2.1 or 10.0 m/min. Truing and dressing of the diamond wheels was done each time before a machining test. The depth of cut was 7 to 23 μm/pass. A dynanometer (quartz 3-component Dynanometer, Type 9257BA, Kistler, Switzerland) was used to record the normal and tangential grinding forces. To order to simulate the effect of a diamond grain with the work-piece, scratching test was used. A scratcher (Stylometer, QUAD S/N:38030-VAKG, QUAD Group, USA) provided with a spherical diamond tip with a diameter of 125 μm was used. The normal force, transverse force and acoustic emission were simultaneously recorded during scratching test.

The ground specimens were heat-treated at 1100, 1200 or 1300°C for 0 h with a ramping rate of 10°C/min and a cooling rate of 30°C/min to release the surface stresses caused by grinding. The annealed surfaces, the scratches on ground surfaces, and fracture surfaces of four-point-bend samples were examined by field emission SEM (S-4100, Hitachi, Japan), XRD (PW1792, Philips Instrument, The Netherlands) and TEM (Jeol 100 CX II, Japan), respectively.

A four-point flexural strength test was performed by a universal testing system (MTS 810, MTS Co., USA). The testing procedures followed the CNS 12701[16] standard. The cross-head speed of the testing machine was 0.5 mm/min. The upper and lower spans were 10 and 30 mm, respectively.

The dimension of test bars is $3\times4\times36$ mm^3, where the 3 mm is the height. The grinding parameters for the test bars were selected as below. The tensile surface of the test bar was always ground by an #800 diamond wheel in a concentration of 100 (4.4 ct/cm^3). The tangential speed of the wheel and the moving speed of the work-pieces were 1310 and 2.1 m/min, respectively. The depth of cut was 5 μm per pass, and conducted at least four times. To examine the degradation of flexural strength caused by the machining, an electrolytic-in-process-dressing (ELID) process with #2000 diamond wheel in a concentration of 100 (4.4 ct/cm^3) was used to minimize surface processing defects. After machining, the standard test bars were annealed at 1400°C for 0 h with a ramping rate of 10°C/min and a cooling rate of 30°C/min to minimize the amount of monoclinic and rhombohedral phases.

3. Results and discussion

3.1. The morphologies of scratched surfaces

Fig. 1(a) shows a track on the polished Y-TZP surface introduced by scratching with a spherical diamond tip moving at a rate of 0.01 cm/s from left to right with increasing load from 0 to 10 kgf. At very low loads, the interaction is not visible due to elastic recovery. The width and depth of scratching track increase with increasing the load of diamond tip. The interaction mechanism changes from plastic deformation to micro-brittle fracture at point "S1" in Fig. 1(a), and to seriously brittle fracture occurring at point "S2".

Fig. 1(b) shows a higher magnification of the "S1" [in Fig. 1(a)] area, the features of which suggest grains sliding along each other or/and intergranular micro-cracking. Moreover, it is noted that surface chipping is caused by intergranular fracture.

During scratching, the normal force (kgf), transverse force (kgf), and acoustic emission were recorded, as shown in Fig. 2. The normal load smoothly increases with the scratching distance. The loads needed for for the development of brittle fracture are about 4.5 and 6.5 kgf, respectively, at the positions of S1 and S2 shown in Fig. 2(a). The transverse force [Fig. 2(b)] is close to zero in the plastic deformation region, and continuously increases after the S1 point. The acoustic emission signal becomes weaker and smoother after the S1 point, but strong acoustic peaks appear after the S2 point which corresponds to the macro-fracture (chipping) in Fig. 1. The schematic diagram of the contact area of a diamond scratcher and specimen surface is show in Fig. 3. For indentation testing, the contact area can be calculated by the equation:

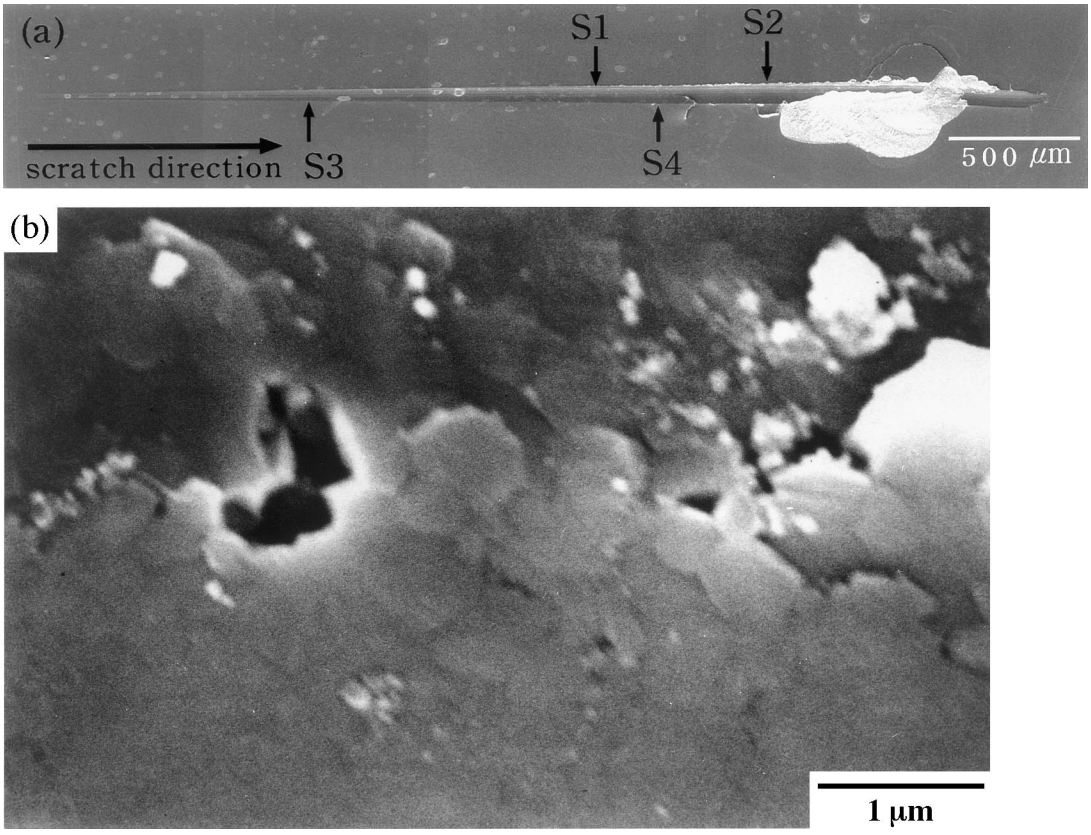

Fig. 1. SEM micrographs illustrating (a) a scratching track on the polished TZP sample, where microcracks appears after S1, seriously brittle fracture starts at S2, S3 and S4 are the place the stresses were calculated, (b) a high magnification of "S1" region.

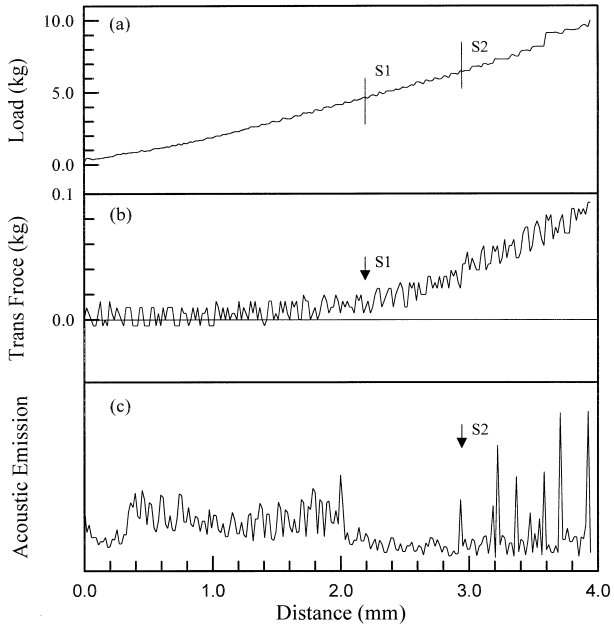

Fig. 2. (a) Normal load, (b) transversal force, and (c) acoustic emission during a scratching test. Note that the S1 and S2 correspond to those in Fig. 1.

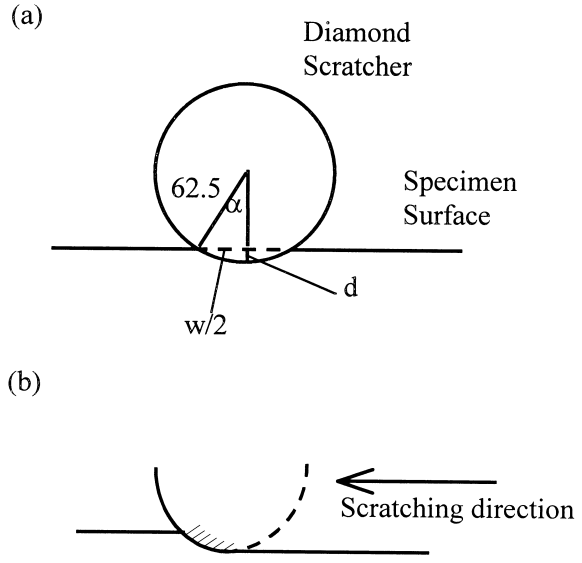

Fig. 3. Schematic diagram of the contact area (a) of a diamond tip indented into the specimen surface, and (b) of diamond scratcher tip and specimen surface.

$$A = 2\pi \cdot 62.5^2 \cdot (-\cos\theta)|_0^{\alpha}$$

However, the contact area during scratching test should be one half of indentation (A). The stresses of positions S1, S2, S3 and S4 can be calculated and list in Table 1. The normal stresses [F_n/(A/2)] and Hertzian stresses [$F_n/(w/2)^2$] were around 22 and 24 GPa at these four places. These results indicate that both normal stress and Hertzian stress keep approximately constant and larger than 12 GPa, the critical Hertzian stress of plastic deformation for ZrO_2,[17] during the test. Therefore, neither normal stress nor Hertzian stress contributes to the brittle fracture and to the change of deformation mechanism, but the transverse stress does. The generation

Table 1
The contact area and normal stresses during scratching test[a]

	Track width w (μm)	α (°)	d (μm)	Contact area (μm^2)	Normal force, F_n (N)	Normal stress (GPa)	Transverse force, F_t (N)	Transverse stress (GPa)	Hertzian stress (GPa)
S1	66.7	32.2	9.6	1890	44.1	23.3	1.96	1.03	25.2
S2	82.1	41.0	15.3	3010	63.7	21.2	3.92	1.30	24.3
S3	46.2	21.7	4.4	870	19.6	22.5	–	–	23.4
S4	71.8	35.1	11.3	2230	49.0	22.0	2.45	1.10	24.2

[a] d is the depth that diamond scratcher indented into the specimen, and α is shown in Fig. 3.

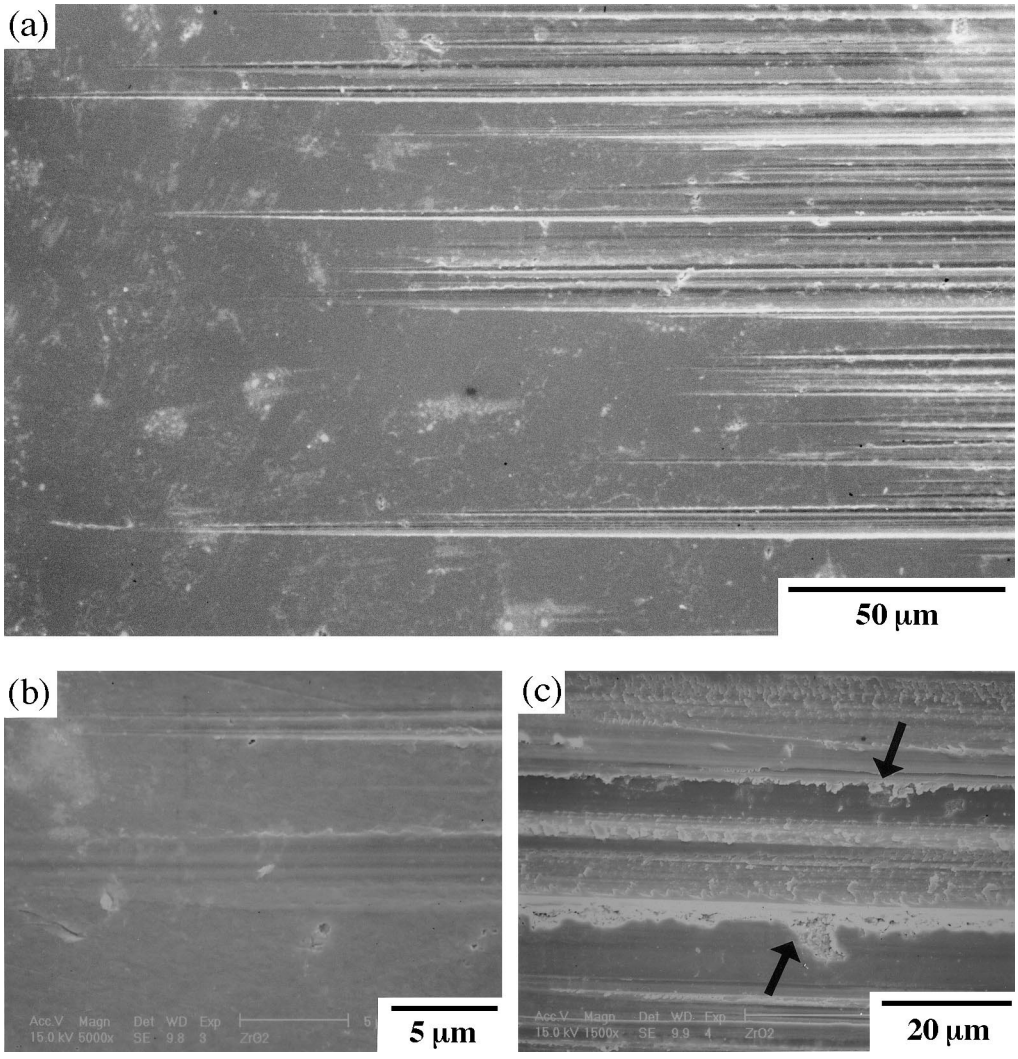

Fig. 4. The ground morphologies of a transition region between polished/ground TZP ceramic by #800 diamond wheel. (a) A general view; (b) the tips; (c) the tracks of a groove.

of acoustic signals [Fig. 2(c)] is the evidence for the formation of cracks during the scratching test.

Fig. 4 shows the features of several parallel grinding tracks on a polished surface (on the left side). The depth of cut is smaller than 5 μm and the morphologies of these tips [Fig. 4(b)] are similar to that of a scratching track in Fig. 1. In the middle of the tracks [Fig. 4(c)], greater normal load and the interaction of the neighbor tracks cause jagged edges and grain pull-out, which results in the removal of the surface layer.

A typical surface morphology of the specimens ground with various wheels is shown in Fig. 5(a). The bottoms of the grooves appear smooth, but the edges are jagged [marked as "j" in Fig. 5(a)]. Besides the jagged edges, perpendicular microcracks [marked as "m" in Fig. 5(a)] appear beside the grooves. The number and the size of bulges and the microcracks decrease with decreasing grit size of the grinding diamond wheel or with table speed. The insert diagram of Fig. 5(b) shows that both longitudinal and transverse surface roughness (R_a) follow the same trend.

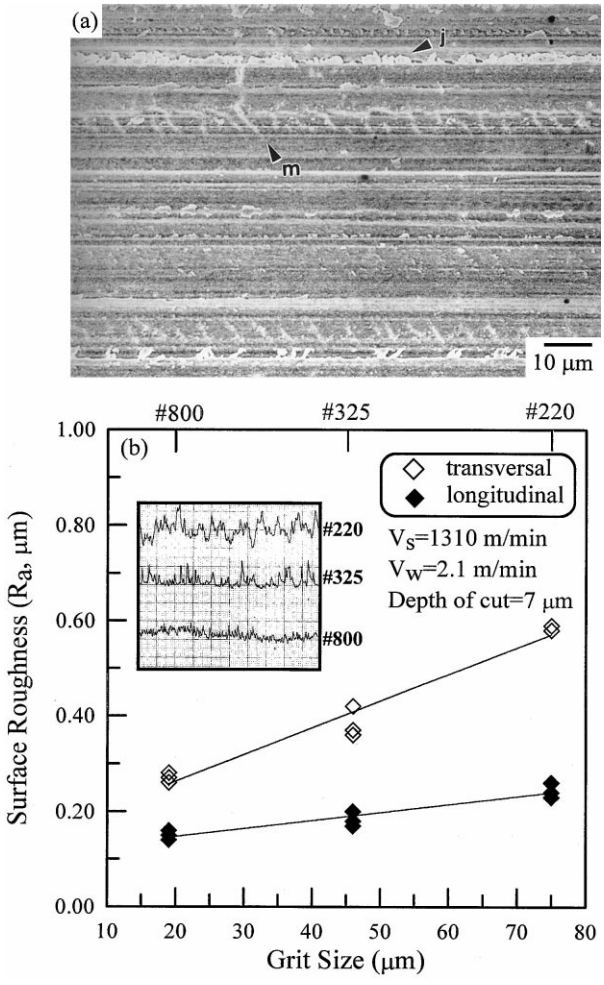

Fig. 5. (a) SEM morphology of the surface ground by a #220 diamond wheel; (b) the surface roughness and profiles of the surfaces ground by either #220. #325 or #800 diamond wheels.

The microcracks on the surface are extending into subsurface. Fig. 6 shows the crack morphologies on the vertical subsurface (fracture surface). There is a machining–processing zone (marked as "c") just under the groove. A semi-circular crack seems to extend from the free surface. The features on TZP resulting from one diamond grain are schematically illustrated in Fig. 6(b). The groove, bulges (b) and jagged edge (j), radial crack (m), processing zone (c), and median crack (d) are indicated. Lateral cracks seldom appear. These microstructural features except for the cracks are produced by plastic deformation exerted by diamond grits.

3.2. The effect on flexural strength

Fig. 7 shows the grinding forces on TZP surface during the machining by a #800 diamond wheel with various depths of cut. The grinding force decreases with a decrease depth of cut and an increase of wheel speed. It is noted that the transversal forces are about half of the normal forces. In other words, the friction coefficient of the wheel grinding on dense TZP is ca. 0.5. The transverse force times the velocity of the diamond scratcher, $F_t{*}V_d$, is the machining energy which may transfer into strain energy, heat or surface energy of newly formed

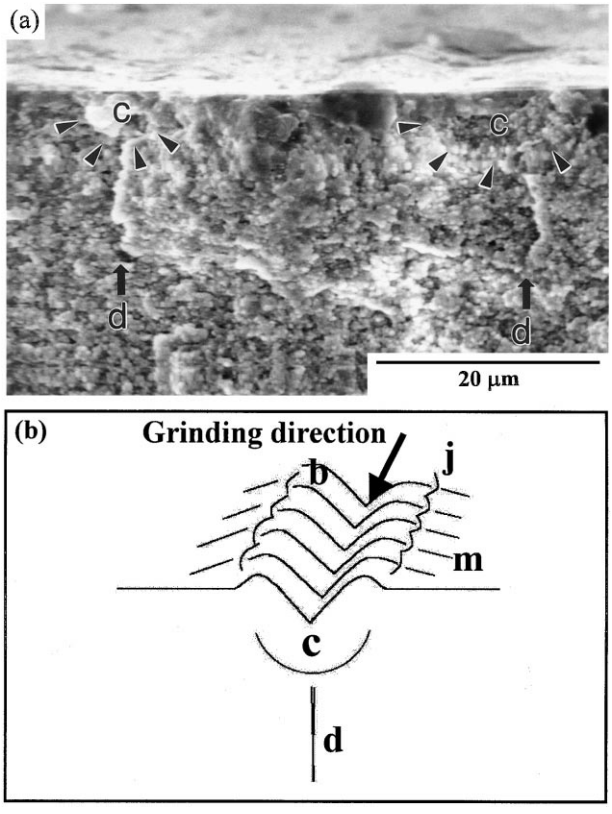

Fig. 6. (a) The morphology of a damaged subsurface ground by a #800 diamond wheel; (b) a schematic diagram of the characteristic features on surface and subsurface introduced by the reaction between diamond grit and TZP specimen.

surface due to microcracks or machining debris. The transversal force is the major factor responsible for the formation of surface radial cracks shown in Fig. 5(a). The cracks are considered as the main defects introduced during machining. It is reported that the flexural strength of ceramics is inversely proportional to the square root of the surface defect size.[18] On the basis of the morphological observation, surface roughness measurements and grinding force analysis, grinding with a #800 diamond wheel and with the depth of cut no greater than 7 μm was selected for the preparation of the test bars for flexural testing.

Processing and machining of TZP are two possible sources of surface defects. Therefore the machining test was conducted on the TZP sample processed from same batch. Two diamond wheels, #800 or #2000 (ELID), were used and the grinding parameters were kept the same. The flexural strength distribution of these specimens is shown in Fig. 8. The distributions and mean strengths for these two machining cases are statistically undistinguishable. Since the diamond grit of #2000 wheel is far smaller than that of #800 wheel, the dimension and frequency of the surface defects caused by a #2000 wheel should be smaller than that caused by a #800 wheel. The average flexural strength shows lightly but not significantly different values. Therefore, a machining procedure with an #800 wheel, small depth of cut (7 μm) and slow table speed (2.1 m/min) is appropriate for the TZP specimens.

3.3. Transformation of crystalline ZrO_2 phase

Phase transformation is an important character of zirconia materials. The XRD patterns of the sample surfaces treated with various conditions are shown in Fig. 9. The results show that the surface of the as sintered materials contained only 3.1% m-phase. During polishing or grinding, the mechanical stresses induce the phase transformation and increase the content of m-phase zirconia to 5.7 and 8.2%, respectively. After annealing at 1200°C for 0 h, m-phase grains reversely transform to t-phase and the amount of m-phase reduces to 2.2%. If the annealing temperature is 1100 or 1300°C, there is 3.3

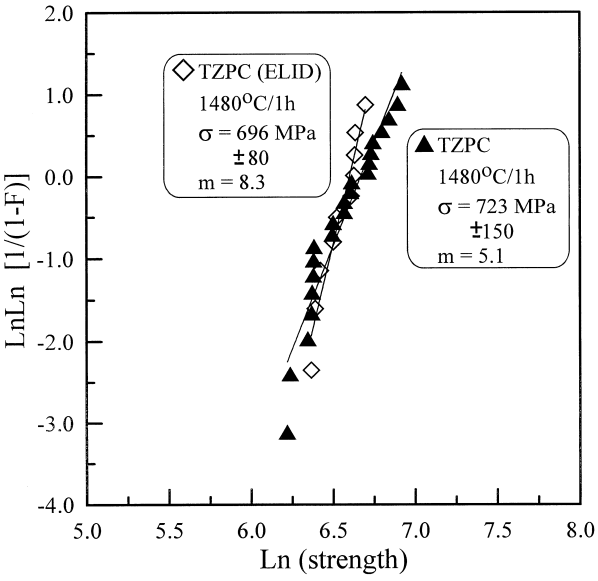

Fig. 8. Statistic results of four-point flexural strength of TZP ground by #800 or #2000 (ELID) diamond wheel.

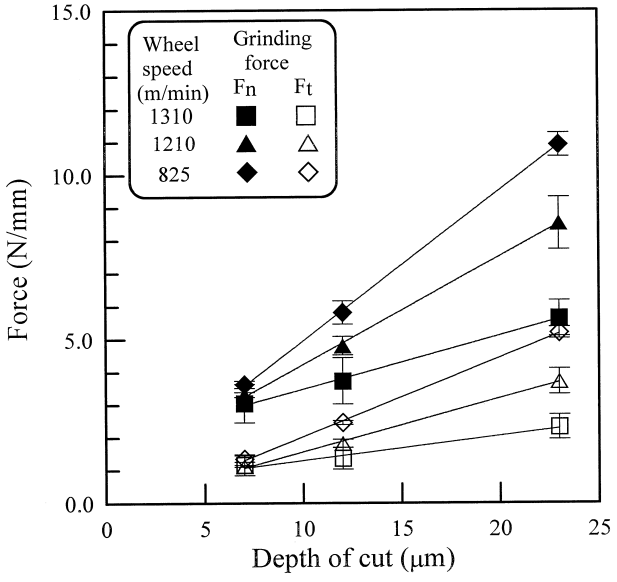

Fig. 7. The normal and transversal grinding forces (F_n and F_t) introduced by machining procedure (#800 wheel).

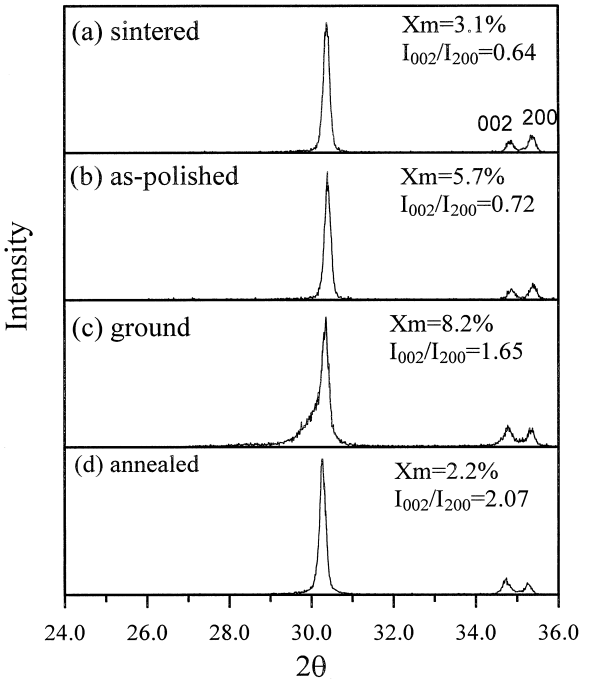

Fig. 9. The XRD patterns of (a) sintered, (b) polished, (c) ground, and (d) annealed TZP specimens.

or 2.1% m-phase, respectively, remained in the TZP. This indicates that the treatment of 1200°C for 0 h is the proper conditions for the recovery of the t-ZrO_2 in TZP.

Besides the t-to-m phase transformation, the formation of a rhombohedral phase on the ground surface was noted. The appearance of $(111)_r$ after grinding results in a non-symmetrical broadening [Fig. 9(c)] of the $(111)_t$ peak. The r-phase can be totally eliminated by heat treatment. The diffraction peak of $(111)_t$ becomes symmetrical again [Fig. 9(d)].

The third effect of grinding process is the formation of FDS which causes the change of the I_{002}/I_{200} ratio, from 0.64 to 2.07 [Fig. 9(a)–(d)]. The FDS occurs after grinding and cannot be eliminated by heat treatment, which is consistent to the reports by other.[15]

3.4. Machining effect on surface microstructure

The grain size of the surface of TZP materials can be refined by a suitable machining/heat treatment process. To show this a dense TZP specimen was polished and thermally etched at 1200°C for 0.5 h. The average grain size and largest grain observed of this specimen are 0.38 and 0.68 μm, respectively. After grinding with an #800 mesh wheel and annealing at 1200°C for 0 h, the results as shown in Fig. 10 are obtained. The average grain size and largest grain of the TZP measured from the micrographs have reduced to 0.15 and 0.28 μm, respectively. A possible explanation is as follows. The surface TZP grains transformed to m-phase or r-phase have acquired strain energy, especially those grains located at bulges on the surface, as shown in Figs. 10(a) and 6(b). Therefore, during the heat treatment, the grain boundaries of the grains are rearranged and recrystallized to reduce the size. The reduction of grain size is caused by the strain energy of plastic deformation during grinding process.[19] The energy offers the driving force of recrystallization.

Machining textures apparently are present on the microstructural scale. Two TEM microstructures of the as-polished and ground/annealed TZP are shown in Fig. 11. Submicrometre grains and fine cracks at grain boundaries are found in the as-polished TZP

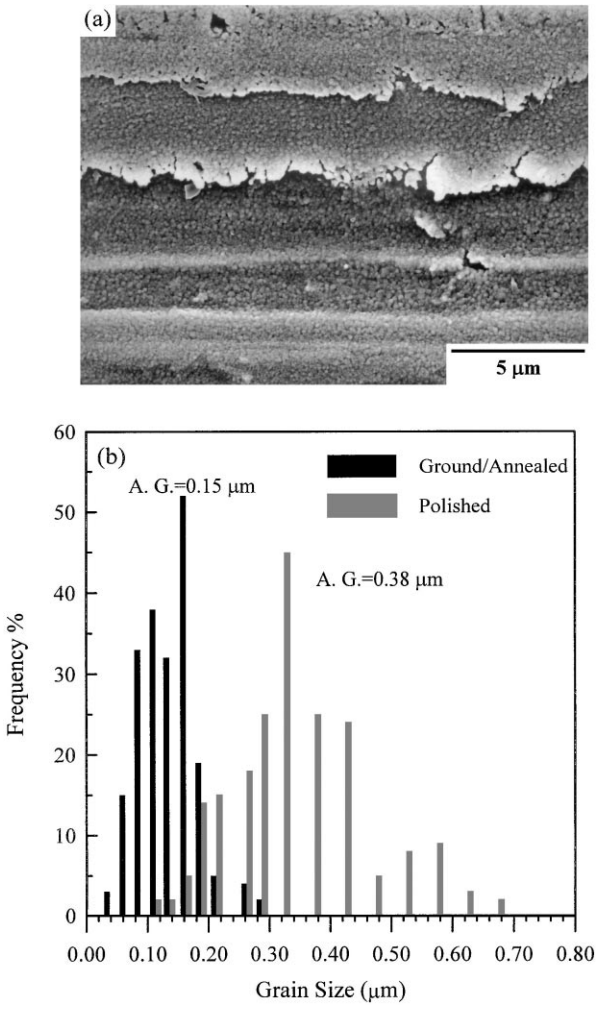

Fig. 10. (a) SEM micrograph of a TZP surface ground by #800 diamond wheel and annealed at 1200°C; (b) the grain size distribution of the TZP before and after machining.

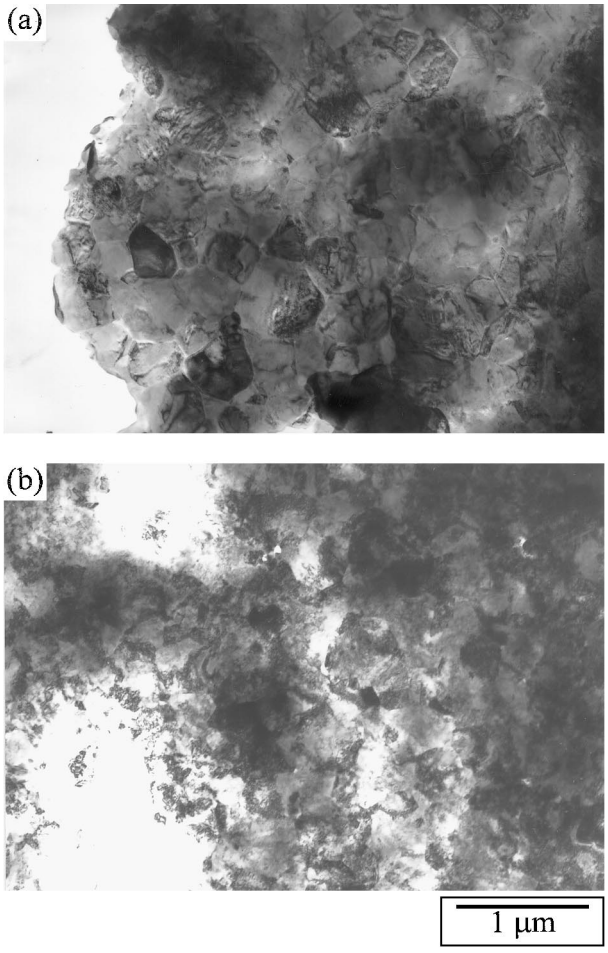

Fig. 11. The bright field image of (a) polished and (b) ground/annealed TZP specimen.

[Fig. 11(a)]. The contrast of the TZP grains is uniform, but not for the ground/annealed sample, which shows multiple contrast of the grain images. Besides, the grain size is apparently reduced and the machining texture (e.g. FDS) still retains after the ground/annealed step [Fig. 10(b)]. Fig. 12 shows two TEM electron diffraction patterns (DP) obtained from the side regions of scratched groove by #800 mesh diamond grit on TZP samples. The crystalline conditions of the TZP grains are depicted by the electron diffraction spots [Fig. 12(a)]. The spots are more diffusive (larger spot size) than those of the ground/annealed specimen [Fig. 11(b)], due to the formation of r-phase and the residual stress by machining. The diffraction spots [Fig. 12(b)] under the same operation conditions (same aperture size and convergent beam angle) are apparently sharper than the previous. The TEM results show that the annealing treatment at 1200°C for 0 h is capable of eliminating r-phase and residual stress, and changes the morphologies of the ZrO_2 grains in the TZP. The evidence supports that the m- and r-phases can be eliminated by heat treatment, but not FDS.

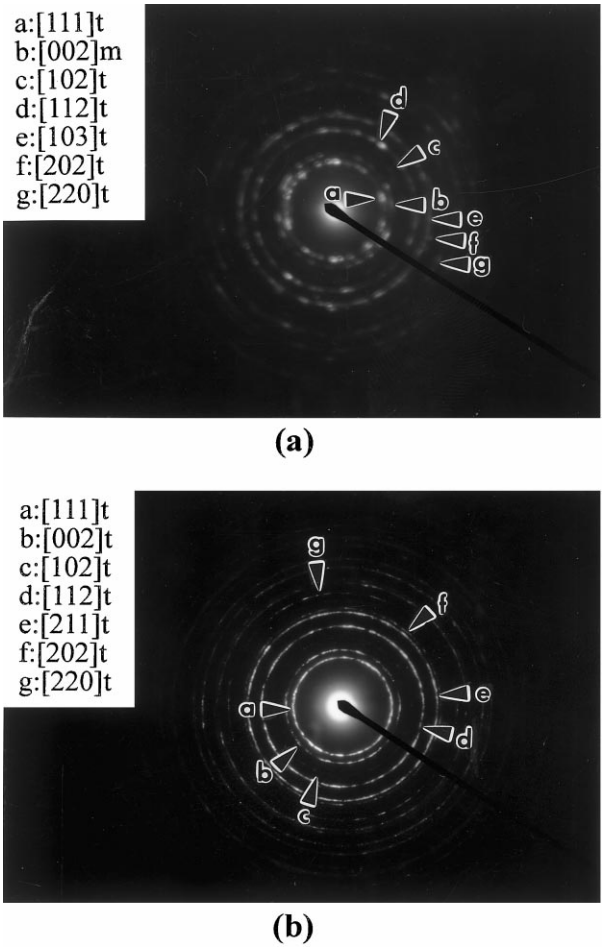

Fig. 12. The diffraction patterns of (a) ground with #800 wheel, and (b) ground/annealed specimens at 1200°C for 0 h at the side of groove.

4. Conclusion

Detailed microstructural analysis of scratched or machined TZP was conducted. Plastic deformation is the dominating mechanism for wheel grinding processes on fine-grain Y-TZP. Since the average normal stress is constant during scratching, transverse stress plays a major role on fracturing state of grinding or scratching by diamond grids.

The grooves of scratching track are mostly smooth. Bulges and jagged edges are observed on the grooves. Radial and median microcracks are formed, as the processing zone is introduced from the surface interaction with diamond tip. The number and size of the radial cracks decrease with the decrease of diamond grit size or/and table speed.

In addition, a rhombohedral phase (r-phase) and ferroelastic domain switching (FDS) are found on ground surface. Heat treatment is capable of eliminating the m- and r-phase resulting from machining, but not the FDS. After machining and annealing, the grain size apparently reduces from 0.38 to 0.15 μm.

The grinding force decreases with the decrease of depth of cut or increase of wheel speed. The results of flexural strength indicate that the machining parameters, #800 diamond wheel grinding, a tangential wheel speed V_s of 1310 m/min, a table speed V_w of 2.1 m/min and a depth of cut of 7 μm are appropriate without reducing the strength of TZP test bars.

Acknowledgements

The authors would like to express their appreciation for the financial support of this research provided by National Science Council (NSC) in Taiwan under the contracts NSC86-2622-E-002-026R and NSC-87-2622-E-002-014. Also, the authors are grateful to acknowledge the kind offering of the Stylometer and discussion with Professors S. C. Lee and C. H. Hsu in Tatung University.

References

1. van den Berg, P. H. J. and de With, G., Strength and residual stress of Mg-PSZ after grinding. *Wear*, 1976, **160**, 301–308.
2. Rice, R. W. and Speronello, B. K., Effect of microstructure on rate of machining of ceramics. *J. Am. Ceram. Soc.*, 1976, **59**(7–8), 330–333.
3. Inasaki, I., Grinding of hard and brittle materials. *Annuals of the CIRP*, 1987, **36**, 463–471.
4. Tonshoff, H. K., Trupold, J., Brinksmeier, E. and Wobker, G., Evaluation of surface layers of machined ceramics. *Annuals of the CIRP*, 1989, **38**, 699–708.
5. Frei, H. and Grathwohl, G., Microstructure and strength of advanced ceramics after machining. *Ceram. Int.*, 1989, **19**, 93–104.
6. Kim, B. A., Ando, K. and Sato, S., Effect of grinding on cracks

and the strength of ceramics. *Fatigue Fract. Engng. Mater. Struct.*, 1994, **17**(2), 187–200.
7. Xu, H. H. K., Jahanmir, S. and Wagn, Y., Effect of grain size on scratch interactions and material removal in alumina. *J. Am. Ceram. Soc.*, 1995, **78**(4), 881–891.
8. Tsukuda, A., Kondo, Y., Kuroshima, Y. and Uematsu, K., Relationship between grinding mechanism and residual cracks in single point Grinding test of alumina ceramics with different grain sizes. *J. Ceram. Soc. Japan*, 1995, **103**(3), 268–273.
9. Kitajima, K., Cai, G. Q., Kumagai, N., Tanaka, Y. and Zheng, H. W., Study of mechanism of ceramics grinding. *Annuals of the CIRP*, 1992, **41**, 367–371.
10. Hakulinen, M., Residual strength of ground hot isostatically pressed silicon nitride. *J. Mater. Sci.*, 1985, **20**, 1049–1060.
11. Tomlinson, W. J. and Newton, R. C., Effect of grinding, lapping and various surface treatment's on the strength of silicon nitride. *Ceram. Int.*, 1990, **16**, 253–257.
12. Hasegawa, H., Rhomboherdral phase produced in abraded surface of partially stabilized zirconia (PSZ). *J. Mater. Sci. Lett.*, 1983, **2**, 91–93.
13. Kim, D. J., Jung, H. J. and Kim, H. J., t→r Phase transformation of tetragonal zirconia alloys by grinding. *J. Mat. Sci. Lett.*, 1995, **14**, 285–288.
14. Virkar, A. V. and Matsumoto, L. K., Ferroelastic domain switching as a toughening mechanism in tetragonal zirconia. *J. Am. Ceram. Soc.*, 1986, **69**(10), C224–C226.
15. Kitano, Y., Mori, Y. and Ishitani, A., Structural changes by compressive stresses of 20 mol%-yttria-stabilized tetragonal zirconia polycrystals. *J. Am. Ceram. Soc.*, 1989, **72**(5), 854–855.
16. Anon., CNS 12701. Method of Test for Flexural Strength (Modulus of Rupture) of High Performance Ceramics. CNS, 1991.
17. Suganuma, M., Spherical and vickers indentation damage in yttria-stabilized tetragonal zirconia polycrystals. *J. Am. Ceram. Soc.*, 1999, **82**(77), 3113–3120.
18. Chiang, Y. M., Birnie III, D. and Kingry, W. D., *Physical Ceramics: Principles for Ceramic Science and Engineering*. John Wiley & Sons, Inc., Canada, 1997.
19. Whalen, P. J., Reidinger, E. and Antrim, R. F., Prevention of low temperature surface transformation by surface recrystallization in yttria-doped tetragonal zirconia. *J. Am. Ceram. Soc.*, 1989, **72**(2), 319–321.